Electronic Supplementary Information (ESI) for Chemical Communications. This journal is (c) The Royal Society of Chemistry 2025.
Electronic Supplementary Information (ESI)

Designing a binary sulfides/carbon polyhedron for secondary batteries with high electrochemical and thermal performances

Yongmei Hua[a,#], Fengming Ma[b,#], Jiaqi Gu[e,#], Huizi Songtian[a], Fan Zhou[c], Yang Lu[e], Xiang Fang[d], Lulu Mu[d], Xulai Yang[c], Yin Peng[a,*], Jinjin Li[b,*], Qiye Zheng[e,*] and Jinyun Liu[a,*]

[a] Key Laboratory of Functional Molecular Solids, Ministry of Education, College of Chemistry and Materials Science, Anhui Normal University, Wuhu, Anhui 241002, PR China. E-mail: jyliu@iim.ac.cn (J.Y.Liu); kimipeng@mail.ahnu.edu.cn (Y.Peng)

[b] National Key Laboratory of Advanced Micro and Nano Manufacture Technology, Shanghai Jiao Tong University, Shanghai 200240, PR China. E-mail: lijinjin@sjtu.edu.cn

[c] School of Advanced Manufacturing Engineering, Hefei University, Hefei, Anhui 230069, PR China

[d] Wuhu ETC Battery Co., Ltd, Wuhu, Anhui 241000, PR China

[e] Department of Mechanical and Aerospace Engineering, The Hong Kong University of Science and Technology, Hong Kong SAR, PR China. E-mail: qiyezheng@ust.hk

[#] These authors contribute equally to this work.

Experimental

Materials and reagents: $CuSO_4 \cdot 5H_2O$ and oxalic acid were purchased from Sinopharm Chemical Reagent Co., Ltd., Potassium hexacyanocobaltate ($K_3[Co(CN)_6]$) were purchased from Aladdin. China. All chemicals were used directly without further purification.

Synthesis of Cu/Co-PBAs: Bimetallic Cu/Co-PBAs were synthesized using a co-precipitation method at room temperature. Solution A was prepared by dissolving copper(II) sulfate (3 mmol) and oxalic acid (1.8 g) in deionized water (50 mL). Potassium hexacyanocobaltate ($K_3[Co(CN)_6]$, 2 mmol) and oxalic acid (1.8 g) were dissolved in

deionized water (50 mL) to form solution B. Solutions A and B were separately stirred for 1 h before mixing. Then, solution A was quickly added to solution B, and the mixed solution was vigorously stirred for 6 h. A blue precipitate (Cu/Co-PBA) was obtained, which was centrifuged and washed with deionized water and ethanol several times, followed by drying overnight in an oven at 60 °C.

Synthesis of $Cu_7S_4/Co_9S_8/C$: The as-obtained Cu/Co PBAs and sulfur powders were mixed and put in an alumina boat separately at a weight ratio of 1:6. The boat was placed in a tube furnace for sulfurization and carbonization, which were performed at 500 °C for 2 h under Ar/H_2 (95%/5%) gas atmosphere. After natural cooling, the products were collected.

Characterization: The phase of the sample was determined by using an X-ray diffractometer (XRD, SMART APEX II Brook, copper target). The morphology was observed by field emission scanning electron microscope (SEM, Hitachi S-8100), and transmission electron microscope (TEM, HT-7700, TecnaiG220S-Twin). A high-resolution TEM (HRTEM) was used to observe the lattice fringes. Energy dispersive X-ray spectroscopy (EDS) was employed for elemental mapping and studying the elemental distribution. X-ray photoelectron spectroscopy (XPS, Thermo Scientific K-Alpha), thermogravimetric analysis (TGA, Rigaku TG/DTA 8122) and Raman spectroscopy (Renishaw in Via) were used for characterization. Prior to the BET test, the sample was degassed at 120 °C for 3 h in vacuum to remove water adsorbed on the surface, and then physical adsorption isotherms (adsorption-desorption branch) were recorded using a specific surface area tester (ASAP Micromeritics Tristar 2460). X-ray absorption fine structure (XAFS) spectroscopy was performed using a Rapid XAFS HE (Anhui Absorption Spectroscopy Analysis Instrument Co., Ltd.) with a transmission mode under 20 kV and 20 mA. *In-situ* XRD was conducted using a Rigaku Smart Lab SE XRD system coupled with a battery testing system.

Electrochemical measurements: The 70 wt% active materials ($Cu_7S_4/Co_9S_8/C$), 20 wt% acetylene black and 10 wt% polyvinylidene fluoride (PVDF) were mixed in a ratio of 7:2:1.

The nmethylpyrrolidone (NMP) was used as diluent to disperse the mixture. Evenly-mixed slurry was coated on a Cu foil with a thickness of 9 μm, dried in a vacuum oven at 80 °C for 24 h, and cut into 1.2 mm discs. The mass loading of the active material on each electrode was about 1.2 mg cm^{-2}. The counter electrode was sodium, while the diaphragm was fiberglass. The coin cells were assembled in an Ar-filled glovebox. Electrolyte contained 1 M $NaPF_6$ dissolved in diethylene glycol dimethyl ether. The galvanostatical charge discharge was tested on a Neware Battery system. Cyclic voltammetry (CV, 0.1 mV s^{-1} of sweep rate over the range of 0.1–3.0 V) and electrochemical impedance spectroscopy (EIS) measurements were performed on an electrochemical workstation (CHI 660E). For the assembly of full cells, the $Na_3V_2(PO_4)_3$ (NVP) cathode was prepared by mixing home NVP, acetylene black and PVDF with a weight ratio of 8:1:1 in NMP to form a slurry, which was cast onto aluminum foil. The electrode was cut into a size of 2.83 cm^2, and the typical loading of NVP in the cathode was about 1.3 mg cm^{-2}. In the full cell, the fiberglass was also used as diaphragm. The preparation processes were similar to the half cells shown above. The electrolyte was 1 M sodium hexafluorophosphate ($NaPF_6$) in diethylene glycol dimethyl ether.

Computational methods: Density functional theory calculations were carried out to investigate the properties of Cu_7S_4/Co_9S_8 heterostructures using the Vienna ab initio Simulation Package (VASP) with the projector augmented wave (PAW) method. The exchange and correlation functionals were treated by using the Generalized Gradient Approximation (GGA) in the scheme of Perdew-Burke-Ernzerhof (PBE). The cutoff energy was set at 520 eV for the plane-wave extension of the wave function. The convergence criteria of geometric optimization were set to 10^{-5} eV in energy and 0.02 eV $Å^{-1}$ in force. The 2 × 1 × 1 Monkhorst-Pack k-point meshes were used for geometric optimization. To properly evaluate the weak interaction at the interface, the DFT-D3 method with Becke-Jonson damping was chosen to deal with the van der Waals (vdW) correction. A vacuum layer of at least 20 Å was used to avoid the interactions between the periodic images in the *Z*-axis direction.

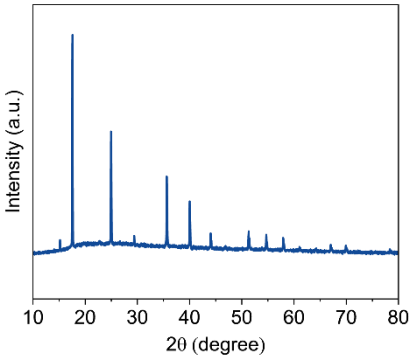

Fig. S1 XRD pattern of the Cu/Co-PBA precursor.

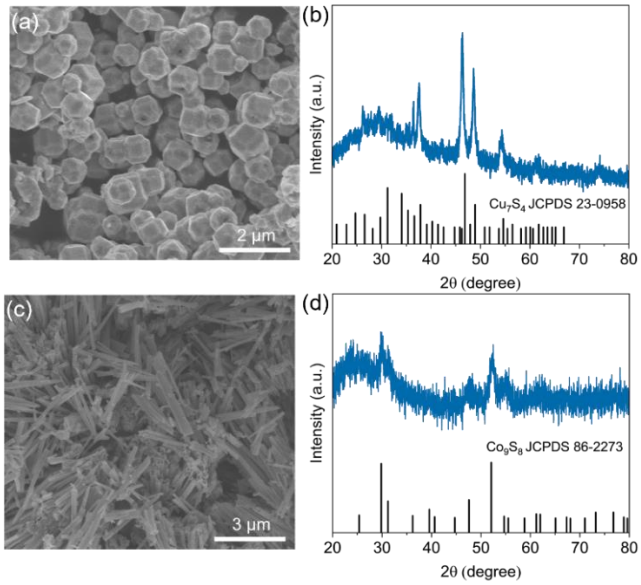

Fig. S2 (a) SEM image and (b) XRD pattern of Cu_7S_4/C. (c) SEM image and (d) XRD pattern of Co_9S_8/C.

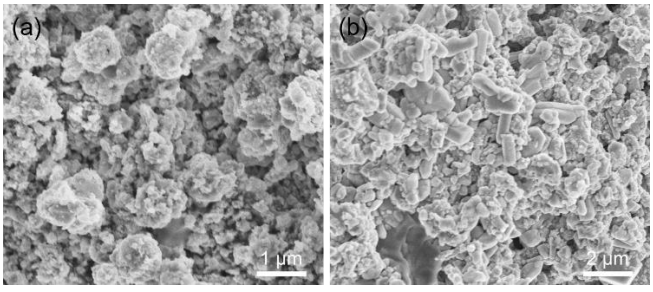

Fig. S3 The sample synthesized by Cu^{2+} and Co^{3+} in molar ratios of (a) 1:2 and (b) 1:3.

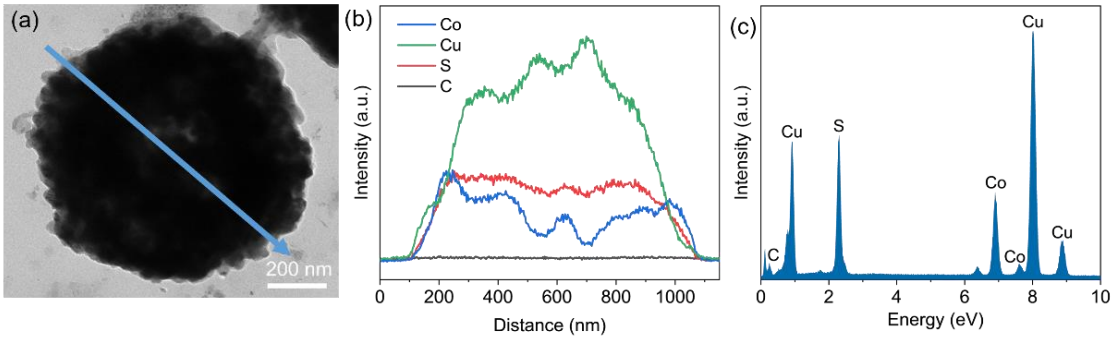

Fig. S4 (a) SEM image, (b) line-scanning curves, and (c) EDS spectrum of $Cu_7S_4/Co_9S_8/C$.

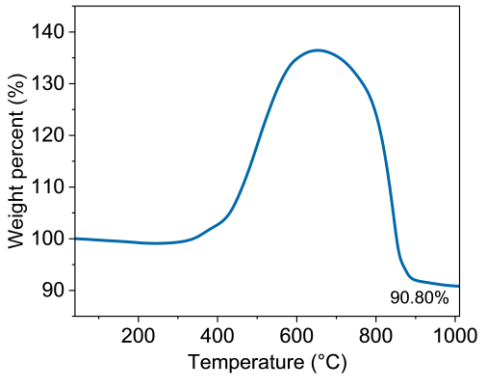

Fig. S5 TGA curve of $Cu_7S_4/Co_9S_8/C$.

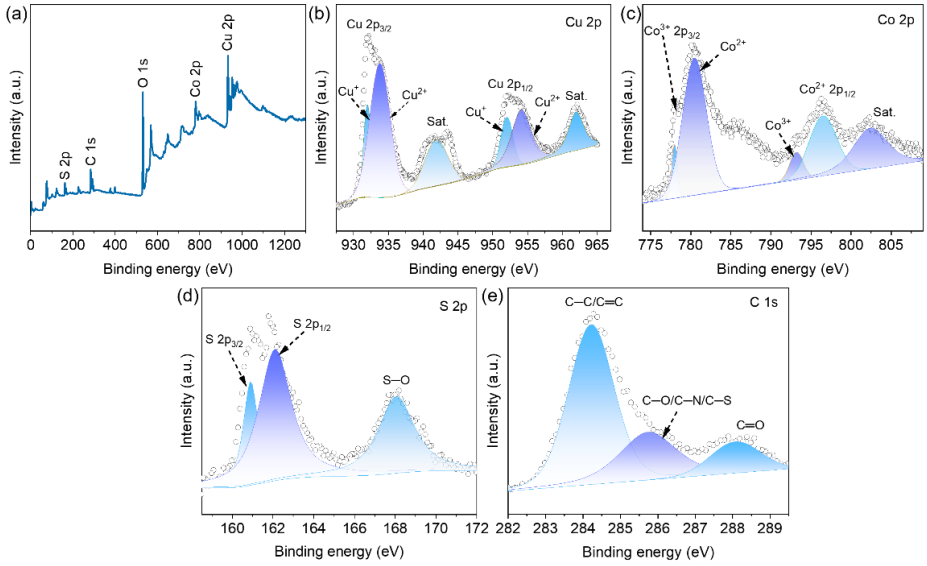

Fig. S6 (a) Survey spectrum, (b) Cu 2p, (c) Co 2p, (d) S 2p, and (e) C 1s XPS spectra of $Cu_7S_4/Co_9S_8/C$.

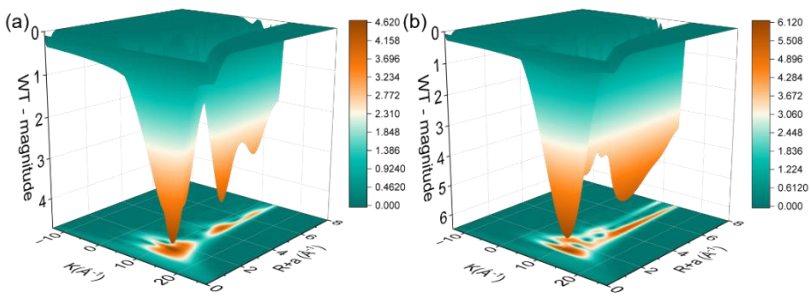

Fig. S7 Wavelet-transform-EXAFS (WT-EXAFS) of $Cu_7S_4/Co_9S_8/C$ at the (a) Cu and (b) Co L_3-edges.

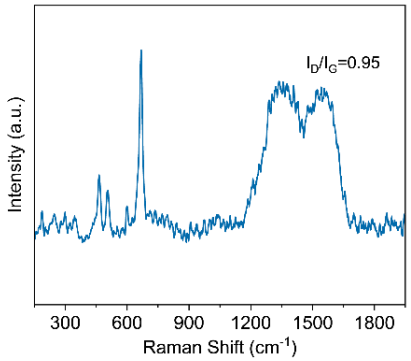

Fig. S8 Raman spectrum of $Cu_7S_4/Co_9S_8/C$.

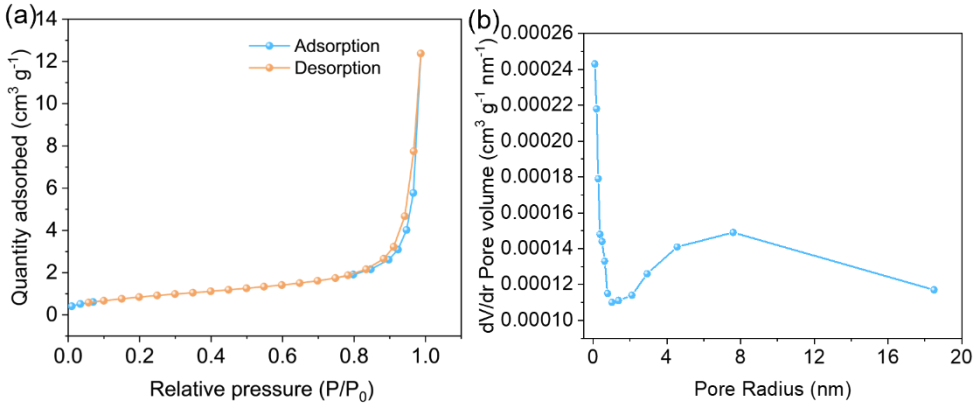

Fig. S9 (a) N_2 adsorption-desorption isotherms and (b) pore-size distribution of $Cu_7S_4/Co_9S_8/C$.

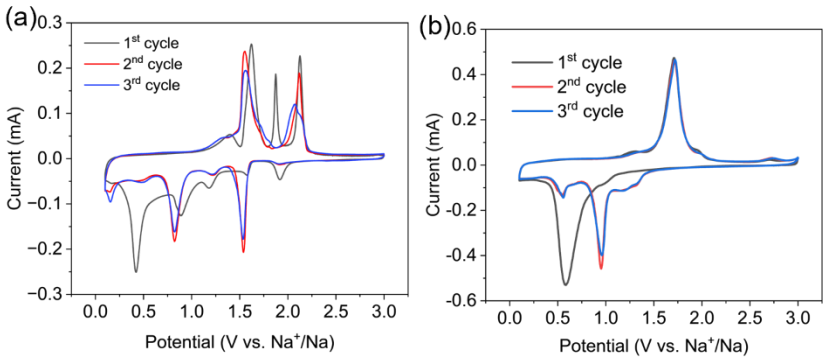

Fig. S10 CV curves during the initial three cycles at 0.1 mV s^{-1}: (a) Cu_7S_4/C and (b) Co_9S_8/C.

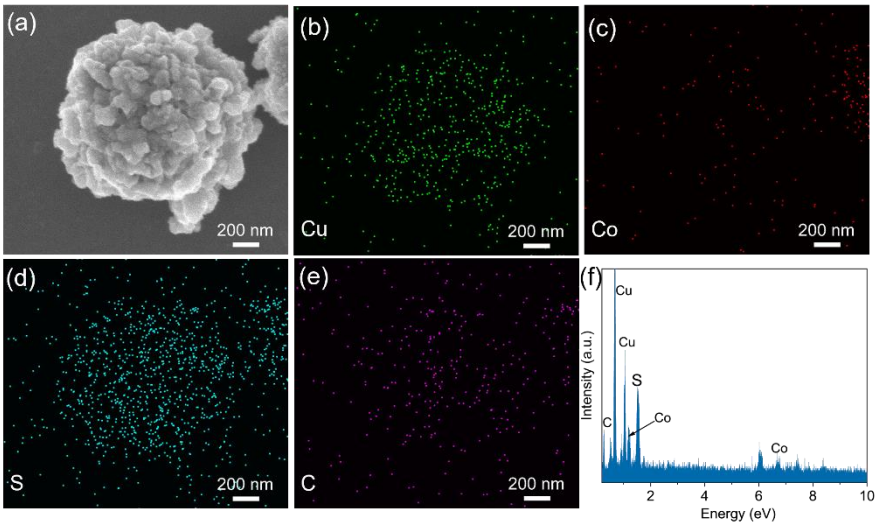

Fig. S11 (a) SEM image, (b-e) the corresponding elemental mappings and (f) EDS spectrum of Cu_7S_4/Co_9S_8/C after cycling 100 times at 3.0 A g^{-1}.

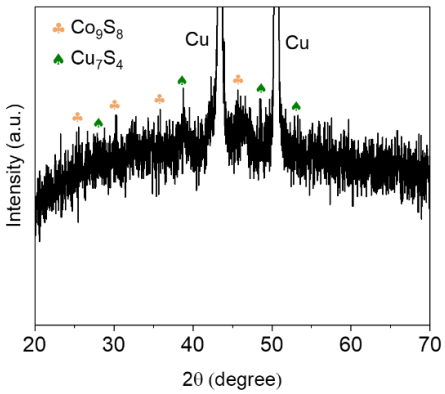

Fig. S12 XRD pattern of Cu_7S_4/Co_9S_8/C after cycling 100 cycles at 3.0 A g^{-1}.

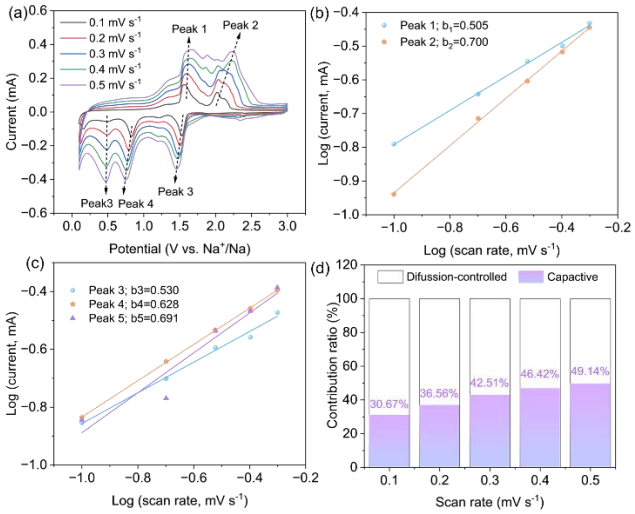

Fig. S13 (a) CV curves of Cu_7S_4/C anode at scanning rates from 0.1 to 0.5 mV s^{-1}. (b, c) The log(i) vs. log(v) of oxidization and reduction peaks. (d) Contribution ratio of capacitive and diffusion-control processes.

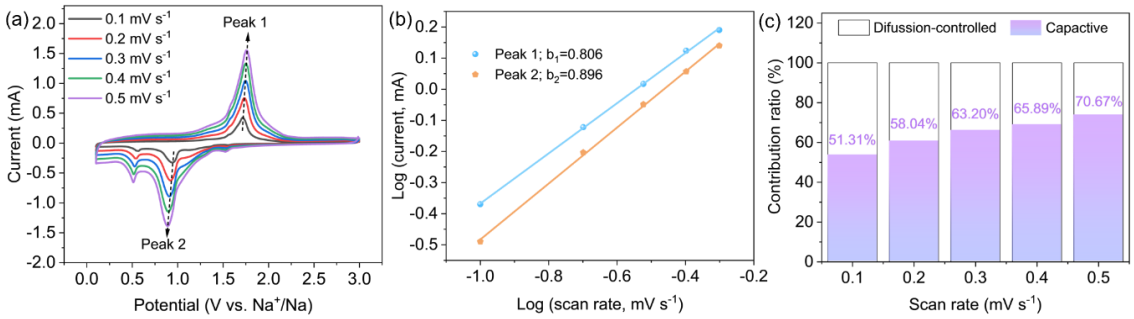

Fig. S14 (a) CV curves of Co_9S_8/C anode at scanning rates from 0.1 to 0.5 mV s^{-1}. (b) The log(i) vs. log(v) of oxidization and reduction peaks. (c) Contribution ratio of capacitive and diffusion-control processes.

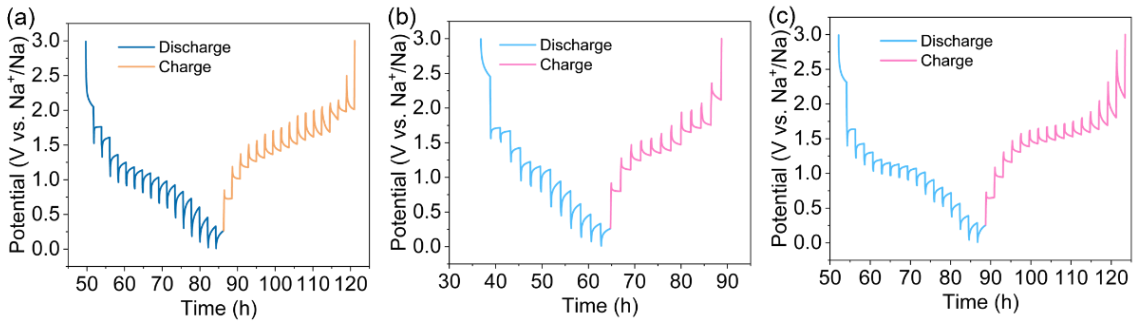

Fig. S15 GITT time-potential distributions of (a) Cu_7S_4/Co_9S_8/C, (b) Cu_7S_4/C and (c) Co_9S_8/C.

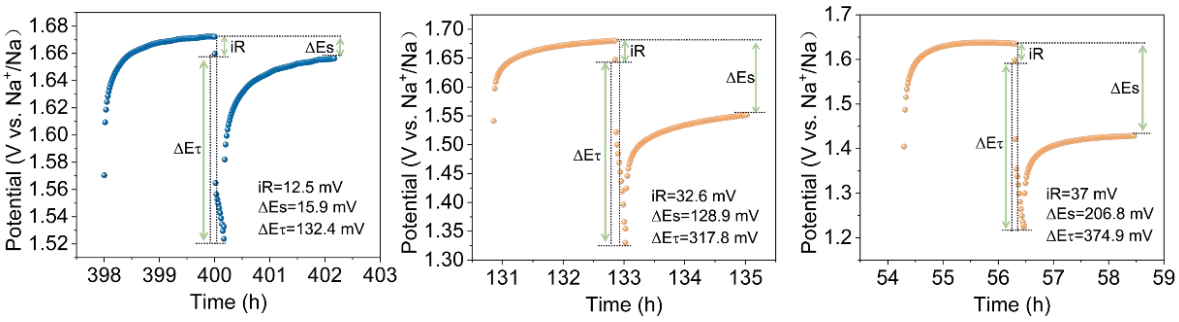

Fig. S16 IR drops of (a) $Cu_7S_4/Co_9S_8/C$, (b) Cu_7S_4/C and (c) Co_9S_8/C.

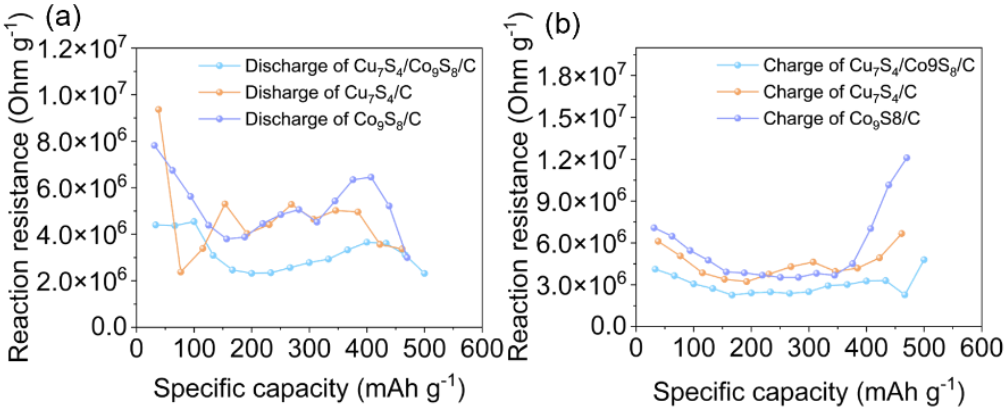

Fig. S17 Reaction resistance of $Cu_7S_4/Co_9S_8/C$, Cu_7S_4/C and Co_9S_8/C during (a) discharging and (b) charging.

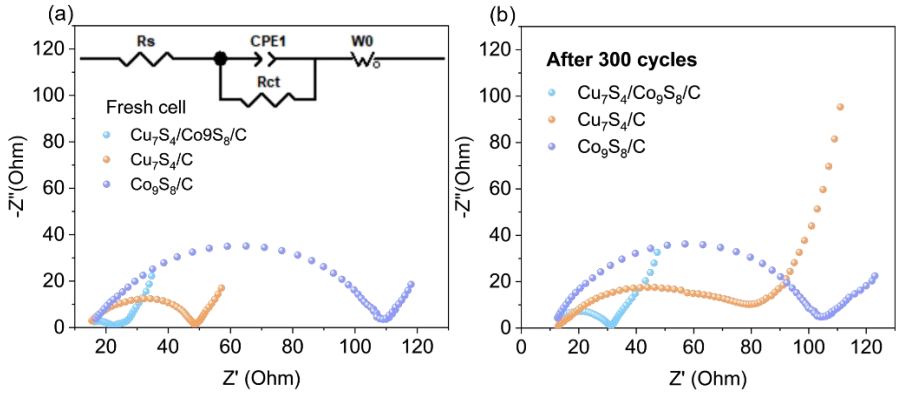

Fig. 18 EIS spectra of $Cu_7S_4/Co_9S_8/C$, Cu_7S_4/C and Co_9S_8/C (a) before and (b) after 300 cycles at 3.0 A g^{-1}.

Table S1. Bond distances and coordination numbers for $Cu_7S_4/Co_9S_8/C$. Information obtained from EXAFS K and R space transformations with fitting. The low R factors confirm the quality of the fitting.

samples	path	C.N.[a]/N	R (Å)[b]	σ^2 (x 10^{-3} Å^2)[c]	R−factor[d]
$Cu_7S_4/Co_9S_8/C$	Cu-S	2.0	2.17	2.12	0.020
	Co-S	2.0	2.49	2.82	0.021

[a] Coordination number.

[b] Bond distance.

[c] Debye−Waller factor.

[d] Sum of squares measure of the fractional misfit.

The accuracies of the above parameters were estimated as CN, ±20%; R, ±1%; σ^2, ±20%.

Table S2. Comparison on electrochemical performance of some Na-ion battery anodes.

Anode materials	Mass loading (mg cm^{-2})	Electrolyte	Current density (A g^{-1})	Capacity (mAh g^{-1})	Cycle number	Ref.
$Cu_7S_4/Co_9S_8/C$	0.9-1.0	$NaPF_6$ + DEGDME	0.5	556	300	This work
			3.0	508	1300	
U-Cu_7S_4@graphite	0.6-1.0	$NaCF_3SO_3$+ TEGDME	0.5	409	2000	[1]
Cu_7S_4/CNF	1.3	$NaCF_3SO_3$+ DEGDME	1.0	553	300	[2]
Co_9S_8/CoS@NC	2.0-2.5	$NaClO_4$+ EC/DEC (1:1) + FEC(5%wt)	1.0	272	300	[3]
Co_9S_8@C-MoS_2	0.8-1.2	$NaPF_6$ + DME	0.2	550	100	[4]
Co_9S_8/SnS@MCNFs	1.0-2.0	$NaPF_6$+ DIGLYME	2.0	225	400	[5]
Co_9S_8@C/CNTs	0.8-1.0	$NaPF_6$+DME	0.5	500	100	[6]
Co_9S_8 nanoparticles encapsulated N,S-codoped CNTs	1.2-1.5	$NaClO_4$+ EC/DEC (1:1) + FEC(5%wt)	1.0	205	400	[7]
ZnS-Sb@C@rGO	0.9-1.2	$NaClO_4$+ EC+FEC(5%)	2	316	1000	[8]

References

1 T. Wang, H. G. Yang and B. G. Lu, Ultra-stable sodium ion battery cathode realized by Cu_7S_4 nanoparticles, *J. Power Sources,* 2018, **399**, 105–114.

2 L. Zhang, Q. Q. Wang, C. C. Qiang, M. Liu, Q. Y. Wang, S. H. Chen, J. Y. Guo and Z. Fang, Fixing Cu_7S_4 nanocrystals on flexible carbon nanotube film for distinguished sodium storage performance, *Chem. Eng. J.,* 2021, **418**, 129489.

3 T. B. Zeng, Q. Q. Chen, Y. H. Ding, X. Z. Xu, D. Feng and D. L. Xie, Multiphase nano Co_9S_8/CoS encapsulated in N-doped carbon for high capacity sodium-ion battery anode, *J. Energy Storage,* 2024, **76**, 109849.

4 S. Wang, X. Pang, D. Huang, M. Zhang, S. Hu, Y. Huang, F. Zheng, H. Wang, Q. Li and Q. Pan, Construction of Co_9S_8@C-MoS_2 heterostructure for fast charging and superior long-term cycling performance of sodium ion batteries, *J. Colloid Interf. Sci.,* 2025, **680**, 398–406.

5 J. J. Dai, B. Murugesan, W. D. Lin, C. Wang, S. Y. Zhang, J. Wu, D. B. Putungan and Y. R. Cai, Construction of Co_9S_8/SnS heterostructures encapsulated in multi-channel carbon nanofibers as long-term stable anodes for sodium-ion batteries, *J. Alloys Compd.,* 2024, **1002**, 175376.

6 X. Y. Ma, X. Y. He, L. Yu, N. Ahmad, Z. Z. Tao, Z. X. Jiang, J. C. Liang, S. Y. Zeng, L. Shi and G. Q. Zhang, Enhancing ion adsorption capability through the strong interaction in Co_9S_8-carbon hybrids achieves superior sodium ion storage, *Batteries Supercaps,* 2024, **7**, e202400170.

7 H. N. Jia, P. Su, J. H. Fan, T. T. Guo, Y. M. Zhang, L. F. Miao, L. Wan, P. H. Yang and M. C. Liu, Constructing Co-N-C coordination in Co_9S_8 embedded N,S-codoped carbon nanotube as an advanced electrode for supercapacitor and Na-ion battery, *J. Colloid Interf. Sci.,* 2024, **659**, 974–983.

8 S. Y. Cao, Q. M. Liu, H. Y. Chen, G. H. Li and H. J. Zhu, Quadra layer core-shell-core-shell structured Co_9S_8@MnS-NC nanorod composites for enhanced sodium-ion batteries, *Electrochim. Acta,* 2023, **459**, 142569.